A multi-PTO Wave Energy Converter for Low Energetic Seas: Ensenada Bay Case

P. Meneses Gonzalez, Edgar Mendoza, Vasiliki Stratigaki, P. Troch, E. Carpintero Moreno

Abstract—**The paper presents a wave energy converter concept to harvest energy at Ensenada Bay, Mexico. The study area can be classified as a low energy sea due to the mean wave power being around 10 kW/m; the wave conditions are significant wave height of 0.5 to 2.5 and peak period of 5 to 20 s. The wave energy converter is formed by a torus buoy and anchored to the sea bottom by four connection structures distributed every 90°. The connected structures play a piston role, and their response is leveraged to run a power take-off system, for example, a linear or hydraulic system. This work does not focus on designing the power take-off system; therefore, it is simplified as linear damping, and an iterative process calculates its value. The hydrodynamic buoy study is made on the frequency domain with Nemoh BEM solver and the power absorption on the time domain with the WEC-Sim code. The capture width ratio is used to evaluate the wave energy converter performance and is a key factor in choosing the optimal size. The wave energy converter captures an average of 20% of the available energy and is well-fixed between periods 8 and 16 s. The present study achieves its target: providing a wave energy converter system to operate under site wave conditions.**

Index Terms—**WEC, Low Energy Sea, multi-PTO, Ensenada Bay.**

I. Introduction

THE present population increase results in the increment of energy demands; most of the current energy industry uses no-renewable resources as the primary fuel, and their transformation culminated in greenhouse gas emissions contributing to climate change. In this context, renewable energies have become an option to reduce the dependence on fossil energy, being the most popular geothermal, solar, wind, and ocean energy (waves and currents).

Wave energy is a vast renewable resource with a high energy density, good forecasting level, and less variability than wind energy [1]. Over the last decades, the interest and investment in promoting wave energy converters (WEC) technological development has been raised [2]. Several WECs have been designed and patented [3]; however, due to some factors, they do not get commercialization mature. Some factors are the broad diversity of prototypes, as well as high installation and maintenance costs [4].

At first glance, offshore places seem suitable for energy harnessing, and most of the current technologies have been designed for those conditions, demanding robust WECs to withstand waves and extreme weather. Additionally, offshore places have expensive installation, commission, decommission, and maintenance activities [5]. Therefore, low annual mean wave power conditions, such as the Baltic and Mediterranean seas (3 kW/m [6] and 4 kW/m [7], respectively) in Europe or Mexican Pacific coast (10 kW/m) in America [8,9] become an enticing opportunity to develop and install WECs. Existing WECs can be customized to low energy conditions by downscaling process [10,11]. Another option to harvest energy at low energy conditions is developing specifically designed WECs for those areas; for instance, PeWEC [12], a WEC designed for the Mediterranean Sea conditions.

The present work aims to investigate a WEC concept to operate at Ensenada Bay, located on the Mexican Pacific coast, which has been identified as the most wave-powerful area in Mexico. This study focuses on optimizing hydrodynamic performance and finding the optimal PTO damping for the study area conditions.

II. Materials and Methods

A. Study Area

Several studies have identified the northern part of the Baja California Peninsula, Mexico, like the area with higher wave energy potential [8,9], around 10 kW/m. Most available literature focus on Todos Santos Bay, Ensenada; therefore, there is a massive knowledge about the prevalent ocean conditions over the study area. Todos Santos Bay is a semi-sheltered bay located in the northern part of the Baja California Peninsula, Fig. 1; its wave characteristics result from the interaction of swells from the North and South Pacific Ocean and local wind. According to [13], the site called P in Fig. 1 has the higher mean energy flux (10 kW/m), and its scatter diagram can be observed in Fig. 2. It is clearly noticed that there are no predominant wave conditions; significant wave height (H_s) varies between 0.5 m to 2.5 and peak period (T_p) between 7 s and 14 s.

This work was supported by CONACYT scholarship, number: 824273.

P. Meneses Gonzalez is with Department of Civil Engineering, UNAM-Ghent University Technologiepark 60, 9052 Ghent, Belgium: (e-mail: Paulino.MenesesGonzalez@ugent.be).

Edgar Mendoza is with Engineering Institute UNAM Circuito Exterior s/n, edificio 17, cub. 209, Ciudad Universitaria, 04510, Coyoacán, México: (e-mail: e-mail: EMendozaB@iingen.unam.mx).

Vasiliki Stratigaki is with Department of Civil Engineering, Ghent University Technologiepark 60, 9052 Ghent, Belgium: (e-mail: vicky.stratigaki@ugent.be).

P. Troch is with Department of Civil Engineering, Ghent University Technologiepark 60, 9052 Ghent, Belgium: (e-mail: Peter.Troch@UGent.be).

E. Carpintero Moreno is with Department of Civil Engineering, Ghent University Technologiepark 60, 9052 Ghent, Belgium: (e-mail: Efrain.CarpinteroMoreno@UGent.be).

Digital Object Identifier:
https://doi.org/10.36688/ewtec-2023-paper-211

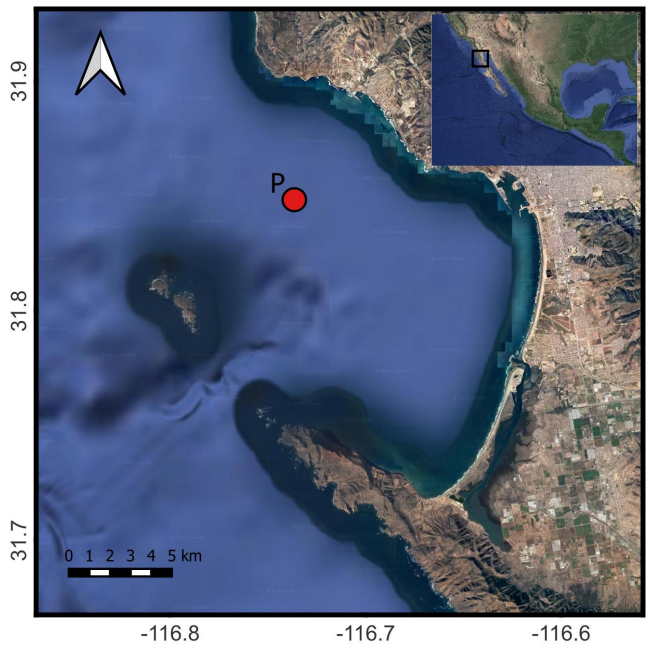

Fig. 1. Todos Santos Bay, according to [13] P is the location with higher potential energy

The bathymetry inside the bay varies between 10 to 100 meters, with the isobath of 20 and 40 meters around 3 and 10 km from the beach.

B. Wave Energy Converter concept

The WEC investigated in this study is based on the Lifesaver concept [14], which consists of a torus floating body (buoy) that reacts to the action of waves. It is anchored to the sea bottom by four connection structures (CS) distributed every 90°. The CS is formed by two built-in cylinder structures that play a piston role moving along the local vertical axis. The CS uses spherical joints at both sides to allow six degrees of freedom buoy motions (Fig. 3). Each CS has a power take-off (PTO) system that activates a generator using the CS linear movement. The PTO system considered in this study is not specified; hence, it is simplified as linear damping. Even though the buoy is released to move in six degrees of freedom, the PTO extracts energy from an equivalent vertical displacement (heave) due to the CS piston movement. The foundation of the CS is assumed rigid and does not allow linear displacement at the bottom. Under uni-directional waves, the problem simplifies to 3 DoF; for instance, considering 0° incident wave direction, the problem reduces to solve the heave-surge-pitch coupling.

In order to assess and optimize the performance of the WEC concept, three torus diameter sizes are evaluated (20 m, 30 m, and 40 m) but with constant cross-section radio (2.5 m). On the other hand, the PTO damping varies to find the optimal values for the operational condition. Fig. 3 shows the WEC concept, and Table 1 the geometric and hydrostatic properties. To restrain the horizontal displacement, the numerical setup includes a horizontal spring acting at the buoy gravity center; the stiffness value was estimated iteratively to limit the buoy movement.

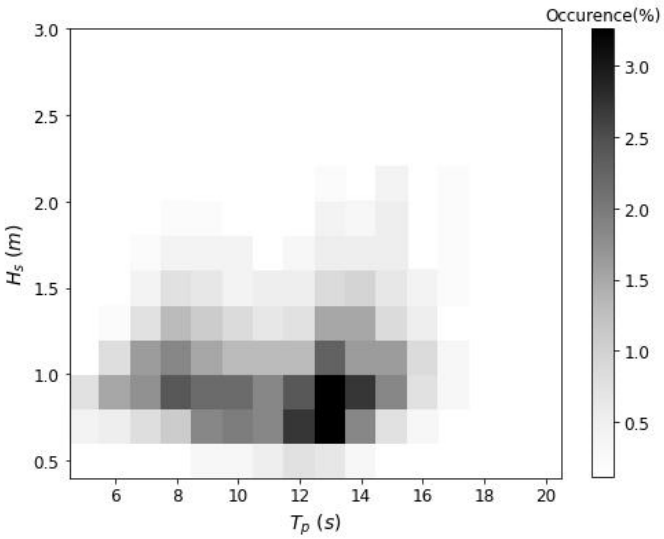

Fig. 2. Scatter diagram for P point [13]. The grayscale represents the ocurrence probability in term of percentage of total hours in a year.

C. Numerical model description

Wec-Sim is an open-source code developed by the National Renewable Energy Laboratory (NREL) and Sandia National Laboratories (Sandia). The code is capable of solving single and multi-body dynamics in the time domain. Additionally, WEC-Sim can include external forces produced by PTO and mooring systems. The code is developed in MATLAB/Simulink (Simscape-Fluids) using the solver Simscape Multibody. A summary of the model equation discretization is presented; however, a complete description is available on its website [15].

The numerical model solves the dynamic response of the system through Equation 1 [16], which uses linear wave theory and assumes waves are the sum of the incident, radiated, and diffracted wave components. The terms in Equation 1 represent a vector with six forces, three translational and three rotational.

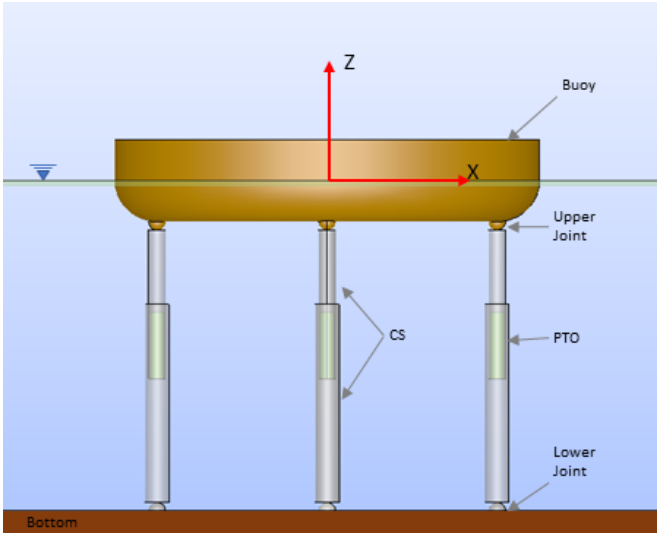

Fig. 3. Wave energy converter concept.

TABLE I
HYDROSTATIC PROPERTIES

Properties	D-20	D-30	D-40
Diameter (m)	20.0	30.0	40.0
Draft (m)	2.5	2.5	2.5
Displacement (ton)	632.3	948.4	1264.5
Ixx (kg -m2)	3.32e+7	1.08e+8	2.52e+8
Iyy (kg -m2)	3.32e+7	1.08e+8	2.52e+8
Izz (kg -m2)	6.46e+7	2.13e+8	4.99e+8
G. center (m)	[0,0,0]	[0,0,0]	[0,0,0]
B. center (m)	[0,0,-1.05]	[0,0,-1.05]	[0,0,-1.05]
H. stiffness [z] (N/m)	3.2e+06	4.7e+06	6.2e+06
R. moment [x] (N/°)	1.6e+08	5.3e+08	1.3e+09
R. moment [y] (N/°)	1.6e+08	5.3e+08	1.3e+09

$$m\ddot{X} = F_{exc}(t) + F_{rad}(t) + F_B(t) + F_{md}(t) + F_{PTO}(t) + F_v(t) + F_{me}(t) + F_m(t) \quad (1)$$

The left side represents the force on the body where $m\ddot{X}$ is the product of body mass and acceleration. The right side is the sum of the acting force over the body. F_{exc}, F_{rad}, and F_B depend on the hydrodynamics coefficients and are solved by the Nemoh BEM solver [17]. F_{exc} is the wave excitation force formed by diffraction and Froude-Kirlov forces. F_{rad} is the wave radiation force, including the added mass and damping terms. F_B is the buoyancy term that depends on the hydrostatic stiffness coefficient (K_{hs}), displacement, and body mass. F_v is the viscous damping force, F_{PTO} is the PTO force, F_{me} is the Morison element (drag forces), and F_m is the mooring force.

D. Numerical setup

The WEC numerical model setup in Simulink can be observed in Fig. 4; the blue and purple block represents the buoy and CS, respectively; they are hydrodynamic bodies, which means their hydrodynamic coefficients were used to solve the system response. A single body simulates each CS, and the equivalent heave movement occurs at the CS top side; this simplifies the model and saves computational time without any effects on results. Yellow blocks represent spherical joints that connect the CS with the buoy and foundation. Red blocks represent the PTO systems conceptually inside the CS but place at the top by simplification. Gray blocks are non-hydrodynamic bodies, and their role is to allow connection between PTO blocks and rotational joint blocks; however, their hydrodynamic properties do not involve solving the system response. The orange block is the horizontal spring acting at the buoy gravity center; its value is 100 kNs/m on the X-axis.

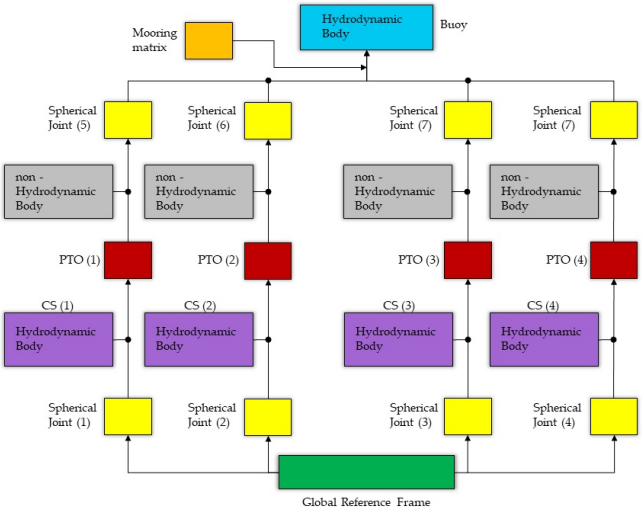

Fig. 4. Numerical model setup in Simulink.

E. Evaluation Parameters

The capture width ratio (CWR) is chosen to evaluate the WEC sizes, and it is the ratio of power captured by the device and the total power flowing through the WEC [18]. Equation 2 shows the CWR formulation, where P is the absorbed power energy, J is the power wave resource, Equation 3, and B is the characteristic dimension. B is calculated by $B = \sqrt{\frac{4A_w}{\pi}}$, with A_w equal to the horizontal cross-section area.

$$CWR = \frac{P}{JB} \quad (2)$$

$$J = \frac{\rho g^2}{16\pi} H_s^2 T_p C_g \quad (3)$$

$$C_g = \frac{1}{2}\left[1 + \frac{2kd}{\sinh(2kd)}\right] \quad (4)$$

C_g is the group velocity, k is the wave number, and d is depth water.

Once the best diameter was chosen, the mean annual energy absorption (MAEA) was evaluated. MAEA result from multiplying bin by bin WEC power matrix and wave occurrence matrix. The MAEA is presented by:

$$MAEA = 8760 \sum_{i=1}^{i=N} P_i F_i \quad (5)$$

where P is the power matrix, F is the wave occurrence matrix, and 8760 is the mean hours per year. The power matrix contains information about the captured energy for each scatter diagram sea state.

III. Results

A. RAOS

The RAOs describe the body's response to wave excitation; RAOs, without PTO force, are calculated under regular wave conditions. Fig. 5 shows the RAOs of the buoy for uncoupled motions; it can be observed that the heave response, Fig. 5a, decreases when the diameter increases, mainly at lower period, converging to a maximum value from 12 s. In contrast, pitch RAOs, Fig. 5b, have larger values at periods lower than 8 s, being the pitch RAO for D-20 larger than the others and decaying to similar values for larger periods.

Fig. 6 shows the total displacement of buoy-CS connection points under regular waves, unitary wave height, and surge-heave-pitch coupling motion. Results are obtained in the time domain, where one spring equal to 100 kN/m is set in the X-direction to keep the oscillated surge motion less than wave height and 0 PTO force. As observed in Fig. 3, CSs are arranged every 90° aligned with X and Y axes. Considering wave propagation in the X direction, the CS on X negative side (bow CS) encounters the incoming wave first, and the rest (middle and stern) experience a lagged response. A similar response between the bow and stern Buoy-CS connection can be noticed in Fig. 6a and 6c. Although the D-30 and D-40 displacements at the bow and stern positions are similar for low periods, both plots tend to separate after 10 s; the D-4O response decreases until it gets less displacement than the D-20 curve, whereas D-30 has the larger response and the difference with the D-20 curve remaining more or less constant. An inverse response at the middle location is observed in Fig. 6b; the curves begin with minor values and increase in function of the period. The middle connections curves are similar to Heave RAOs, and this is due to their location, aligned with the Y axis; the pitch effects are less important than the bow and stern positions. In this case, total displacement is larger for D-20, followed by D-30 and D-40.

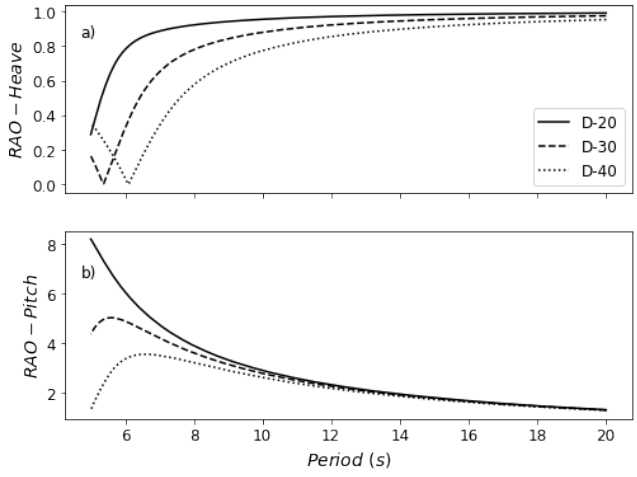

Fig. 5. RAOs. a) uncoupled heave, b) uncoupled pitch.

B. Wave Spectrum

The wave spectrum gives the wave energy distribution among different wave frequencies. Therefore,

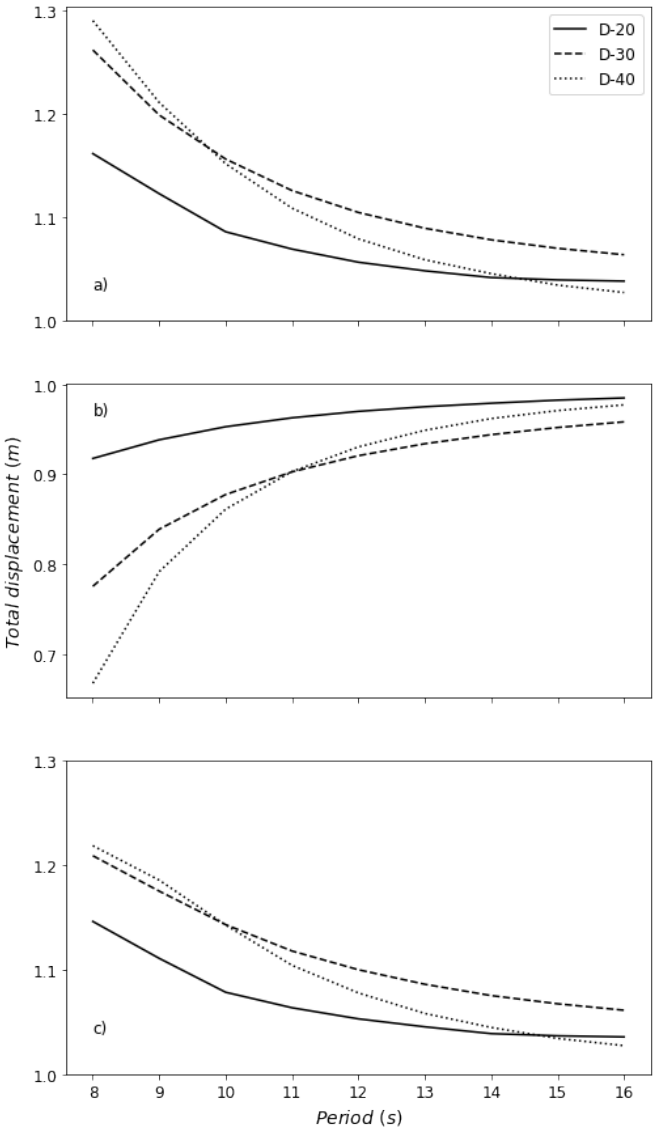

Fig. 6. Total displacement at Buoy-CS conection. a) bow, b) middle and c) stern position.

a good agreement between synthetic and measured wave spectrums is required to force the numerical model correctly. Fig. 7 shows a wave time series of the study area [19]; the data were taken in an area of 20 m depth at a sampling rate of 1 Hz. In order to choose a suitable wave spectrum for the study area, a comparison between the real wave spectrum and three synthetic wave spectrums was made, Fig 8. The real wave spectrum ($JS_{measured}$) was obtained from the time series; $JS_{Goda-1988}$ is the version of the Jonswap spectrum published by [20] and widely applied in the marine engineering community [21]. JS_{IEC} is the Jonswap spectrum integrated into WEC-Sim. It takes into account the gamma (γ) variances (1 - 5) with the relation $T_p/\sqrt{H_{mo}}$, where γ controls the sharpness of the spectral peak, and $H_{mo} \approx H_s$; when gamma is equal to 1 results in Pierson–Moskowitz spectrum. JS_{TMA} is a modified Jonswap spectrum multiplied by a depth-frequency function to consider the shoaling effects when waves propagate into finite depths [22]. The three synthetic wave spectrums were calculated with wave conditions derived from $JS_{measured}$; T_p =

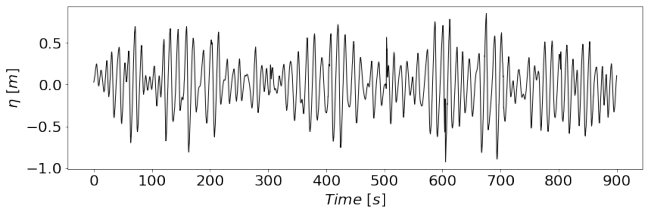

Fig. 7. Surface elevation time series.

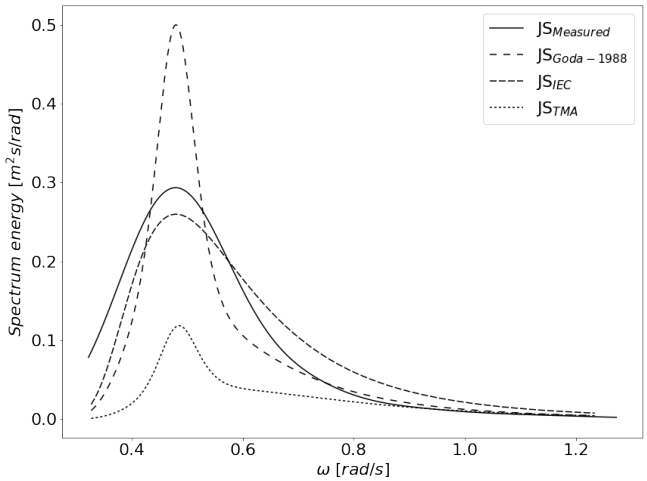

Fig. 8. Wave energy spectrum comparison.

13.1 s and H_s = 1.18 m.

Fig. 8 shows the $JS_{Goda-1988}$ is sharper than spectrum references and overestimates the peak energy value. In contrast, the JS_{TMA} underestimates energy values in the whole spectrum. Meanwhile, JS_{IEC} has a better fit to $JS_{measured}$; therefore, it was used to reproduce the irregular sea surface and force the time-domain numerical model.

C. Theoretical Optimal PTO Damping

As mentioned before, the PTO effects are simplified to linear damping. The theoretical optimal damping (C_{OPT}) for heave motion is calculated by Equation 6 [23], where B is the hydrodynamic damping, m is the torus mass, A the added mass, and ω is the angular frequency. Fig. 9 shows the C_{OPT} for heave response; for the three geometries, the C_{OPT} increases in function the T_p. For the T_p range with significant occurrence probabilities, from 6 to 15 s, C_{OPT} is less than 12 MNs/m; it is the upper limit to estimate the PTO damping under surge-heave-pitch coupling.

$$C_{OPT} = \sqrt{\left(B^2 + \left(\omega\left(m + A\right) - \left(\frac{\rho g S}{\omega}\right)\right)^2\right)} \qquad (6)$$

D. Capture Width Ratio

Capture width energy (CWR) is an index to measure the WEC performance in regular or irregular waves; this study estimates the CWR considering irregular waves and surge-heave-pitch coupling motion in the

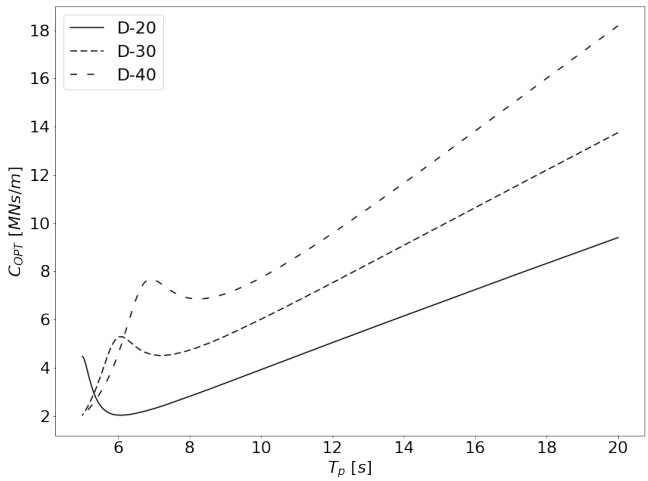

Fig. 9. Theoretical Optimal PTO damping.

damping range of 0.1 - 2.9 MNs/m per PTO. According to [23], the optimal PTO damping for heave WEC is strongly related to wave period and independent of wave height; hence, the CWR is estimated for predominant H_s, 1 m, and period with higher occurrence probability, 12 s. CWR is calculated in the time domain, where captured energy is averaged over 1 hour. Irregular surface elevation is reproduced using Jonswap spectrum [24] and wave energy resource using Equation 3.

Fig. 10 shows the CWR for a period of 12 s as a function of the buoy diameter and PTO damping. The maximum D-20 CWR is 0.23 and happens with 0.9 MNs/m; for D-30 and D-40, the maximum CRWs are 0.27 and 0.29 when damping is 1.3 and 2.1 MNs/m, respectively. The peak CWRs increment 17% and 26%, D-30 and D-40, concerning D-20; on the other hand, the PTO damping increase 44% and 133 %, respectively. Based on CWR and the total displacement, the suitable diameter buoy is 30 m, and the optimal PTO damping is 1.3 MNs/m per PTO. Fig. 11 shows the surface elevation and power absorption for the geometry and damping chosen. Fig. 12 shows the maximum CWR is 0.36, and it happens between T_p of 6 - 10 s. Table 2 compares the current CWR values and CWR database [18] for devices with heave working principle. The current CWR is in the range of previously developed WECs but in significant low wave energy conditions.

E. Power Matrix and mean annual power absorption

The power matrix is shown in Fig. 13; the maximum power is observed for H_s over 2 m and T_p between 8 and 14 s. Power matrices with a similar form can be found in previous studies [25], mainly related to heave absorbers, which is the typical response of that sort of WEC; however, the premise of this study is to present a WEC concept to absorb energy at longer periods and small wave heights.

Fig. 14 is the performance matrix for the site wave conditions; mean power absorption per year for each sea state is between 2 to 8 MW; the values are scattered mainly throughout the T_p, and under 2.0 m of H_s. The total mean annual power absorption is equal to 304 MW.

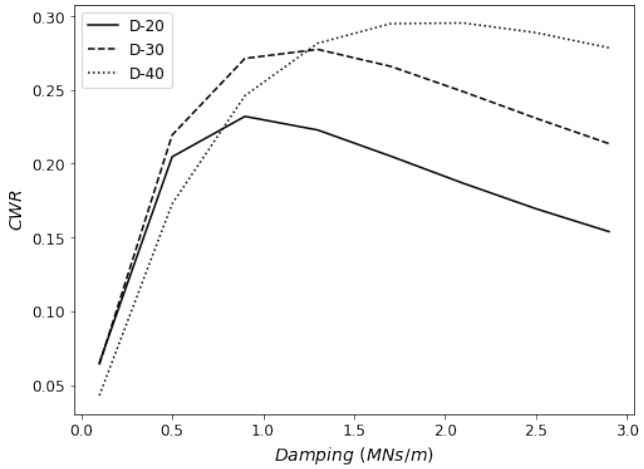

Fig. 10. Capture width ratio for $T_p = 12\ s$.

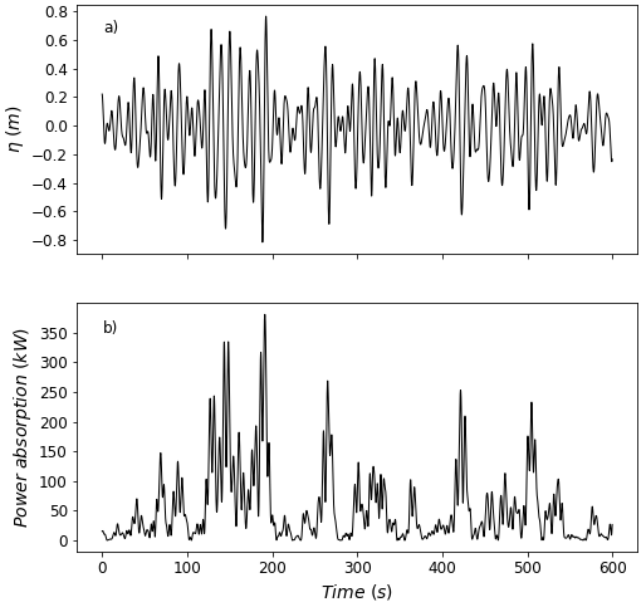

Fig. 11. a) Surface elevation, b) power absorption for $H_s = 1$ m, and $T_p = 12$ s.

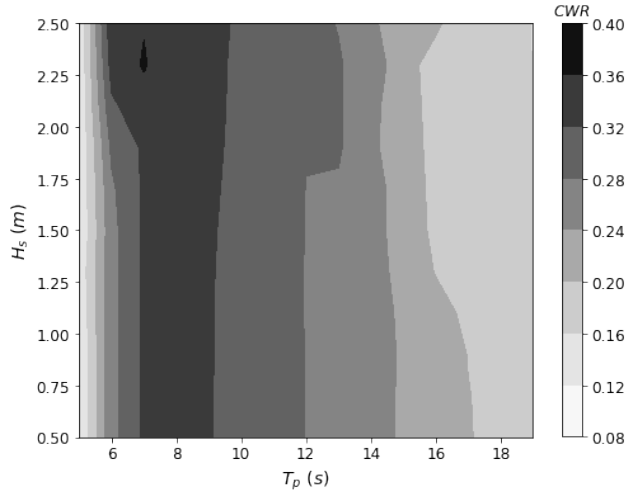

Fig. 12. CWR contours. CWR mean= 0.25.

To compare the improvement between surge-heave-coupling and pure-heave response, the pure-heave

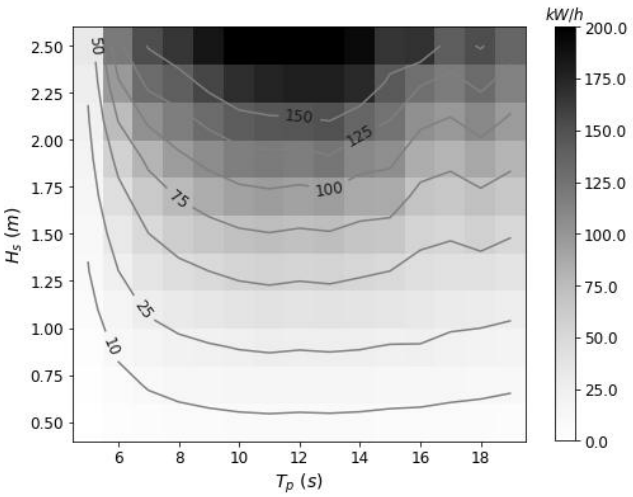

Fig. 13. Surge-heave-pitch coupling response power matrix.

power matrix is presented in Fig. 15. On this condition, the higher potential region becomes small and moves to higher T_p and H_s. Additionally, the maximum value decreases by 30%. The performance matrix, Fig. 16, shows a similar form to the coupling surge-heave-pitch, but the peak value is 25% less, and the total mean annual energy absorption is 202 MW.

IV. Conclusion

The paper presents a location with low to moderate energy sea states with a mean energy flux of around 10 kW/m. A WEC concept is proposed and numerically studied under regular and irregular waves. The study is carried out in frequency and time domains with the

TABLE II
Captured wave ratio

Device	Resource (kW/m)	Sea (H_s/T_p)	CWR
AquaBuoy	12.0 – 26.0	1 – 5.5 m 6 – 17 s	0.10 – 0.26
Wavebob	12.0 – 26.0	1 – 7.0 m 4 – 16 s	0.40 – 0.51
F-2HB	15.0 – 37.0	1 – 7.0 m 4 – 16 s	0.27 – 0.36
B-HBA	13.0 – 34.0	-	0.12 – 0.17
LifeSaver	26.0	-	0.12
Seadog	12.0 – 26.0	-	0.16 – 0.24
Inspired Wavestar	10.0	-	0.10 – 0.15
RM3	34.0	-	0.16
Current study	10.0	0.5 –2.5 m 6 – 17 s	0.16 – 0.36

BEM solver Nemoh and WEC-Sim code, respectively. The frequency domain is used to understand the uncoupled buoy response, whereas the coupling surge-

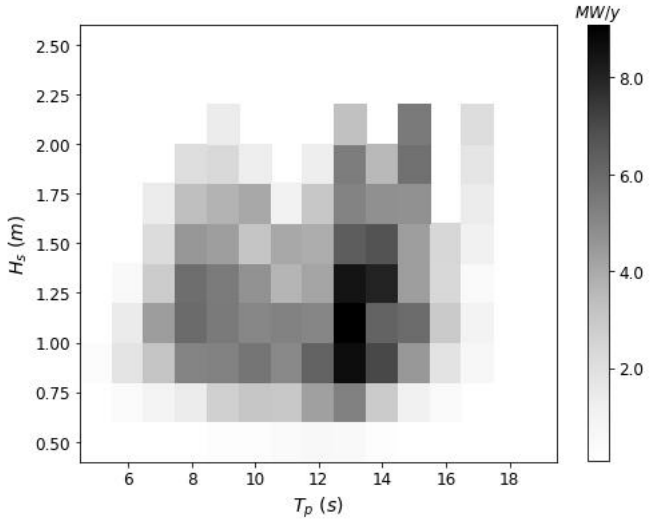

Fig. 14. Surge-heave-pitch coupling response performance matrix. Total mean annual energy absorption = 304 MW.

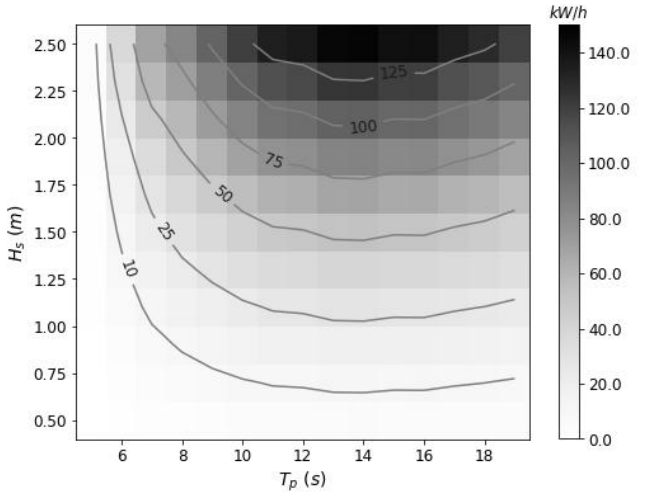

Fig. 15. Heave response power matrix for.

heave-pitch and PTOs effects are simulated in the time domain.

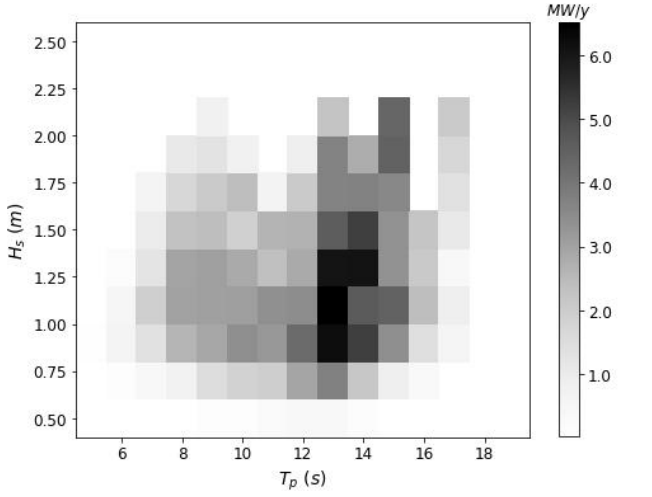

Fig. 16. Heave response performance Matrix. Total mean annual energy absorption = 202 MW.

RAOs indicate the uncoupled heave response decrease when the diameter of the buoy increases and have a larger response at higher periods. In contrast, for uncoupled pitch response, the maximum values reach at low periods, decreasing at higher, and its resonant point move to big periods with major buoy diameter. Once the buoy is released to respond in surge-heave-pitch, CS connection points at the bow and stern positions show a larger response than the middle; due to pitch contribution being more important at those locations.

The CWRs demonstrate that the optimal WEC configuration comprises a diameter of 30 m and damping 1.3 MNs/m per PTO. The WEC concept, under the current assumptions, captures on average 25% of the available wave energy in the study area. The mean annual absorbed energy is 304 MW, representing the mechanical power available to convert into electricity, and the final harvest energy depends on the PTO mechanical system.

Release the buoy response to the coupling surge-heave-pitch improves the power absorption by around 50% compared with the pure-heave response; this is consistent with [26], two or three modes of motion have the potential to harvest more energy.

Finally, the paper achieves the outline; however, in order to get a complete understanding of the WEC concept. Further research should be done on the following points:

1) Influence of wave-current interaction on the WEC dynamics.
2) Design a PTO system to operate efficiently with the WEC concept.
3) Design an efficient mooring system.

REFERENCES

[1] S. Foteinis, J. Hancock, N. Mazarakis, T. Tsoutsos, and C. Synolakis, "A comparative analysis of wave power in the nearshore by wam estimates and in-situ (awac) measurements. the case study of varkiza, athens, greece," *Energy*, vol. 138, pp. 500–508, 2017.

[2] A. F. d. O. Falcão, "Wave energy utilization: A review of the technologies," *Renewable and sustainable energy reviews*, vol. 14, no. 3, pp. 899–918, 2010.

[3] S. Foteinis and T. Tsoutsos, "Strategies to improve sustainability and offset the initial high capital expenditure of wave energy converters (wecs)," *Renewable and Sustainable Energy Reviews*, vol. 70, pp. 775–785, 2017.

[4] R. Ahamed, K. McKee, and I. Howard, "Advancements of wave energy converters based on power take off (pto) systems: A review," *Ocean Engineering*, vol. 204, p. 107248, 2020.

[5] S. Foteinis, "Wave energy converters in low energy seas: Current state and opportunities," *Renewable and Sustainable Energy Reviews*, vol. 162, p. 112448, 2022.

[6] S. Naty, A. Viviano, and E. Foti, "Feaseability study of a wec integrated in the port of giardini naxos, italy," *Coastal Engineering Proceedings*, no. 35, pp. 22–22, 2016.

[7] E. Kasiulis, P. Punys, and J. P. Kofoed, "Assessment of theoretical near-shore wave power potential along the lithuanian coast of the baltic sea," *Renewable and Sustainable Energy Reviews*, vol. 41, pp. 134–142, 2015.

[8] A. Felix, E. Mendoza, V. Chávez, R. Silva, and G. Rivillas-Ospina, "Wave and wind energy potential including extreme events: A case study of mexico," *Journal of Coastal Research*, no. 85 (10085), pp. 1336–1340, 2018.

[9] J. V. Hernández-Fontes, A. Felix, E. Mendoza, Y. R. Cueto, and R. Silva, "On the marine energy resources of mexico," *Journal of Marine Science and Engineering*, vol. 7, no. 6, p. 191, 2019.

[10] A. Majidi, B. Bingölbali, A. Akpınar, G. Iglesias, and H. Jafali, "Downscaling wave energy converters for optimum performance in low-energy seas," *Renewable Energy*, vol. 168, pp. 705–722, 2021.
[11] G. Lavidas and K. Blok, "Shifting wave energy perceptions: The case for wave energy converter (wec) feasibility at milder resources," *Renewable Energy*, vol. 170, pp. 1143–1155, 2021.
[12] N. Pozzi, G. Bracco, B. Passione, S. A. Sirigu, and G. Mattiazzo, "Pewec: Experimental validation of wave to pto numerical model," *Ocean Engineering*, vol. 167, pp. 114–129, 2018.
[13] E. Gorr-Pozzi, H. García-Nava, M. Larrañaga, M. G. Jaramillo-Torres, and M. G. Verduzco-Zapata, "Wave energy resource harnessing assessment in a subtropical coastal region of the pacific," *Journal of Marine Science and Engineering*, vol. 9, no. 11, p. 1264, 2021.
[14] J. Sjolte, "Marine renewable energy conversion: Grid and off-grid modeling, design and operation," 2014.
[15] "Wec-sim v5.0.1," 2022. [Online]. Available: https://wec-sim.github.io/WEC-Sim/master/index.html
[16] M. Lawson, Y.-H. Yu, K. Ruehl, C. Michelen *et al.*, "Development and demonstration of the wec-sim wave energy converter simulation tool," 2014.
[17] A. Babarit and G. Delhommeau, "Theoretical and numerical aspects of the open source bem solver nemoh," in *11th European wave and tidal energy conference (EWTEC2015)*, 2015.
[18] A. Babarit, "A database of capture width ratio of wave energy converters," *Renewable Energy*, vol. 80, pp. 610–628, 2015.
[19] M. G. Jaramillo-Torres, "Estudio numérico del efecto en el espectro direccional del oleaje ocasionado por la presencia de dispositivos ceo," *Master Thesis, CICESE*.
[20] Y. Goda, *Random seas and design of maritime structures*. World Scientific Publishing Company, 2010, vol. 33.
[21] O. M. Mazzaretto, M. Menéndez, and H. Lobeto, "A global evaluation of the JONSWAP spectra suitability on coastal areas," *Ocean Engineering*, vol. 266, p. 112756, 2022.
[22] S. A. Hughes *et al.*, "The tma shallow-water spectrum description and applications," 1984.
[23] C. J. Cargo, A. R. Plummer, A. J. Hillis, and M. Schlotter, "Determination of optimal parameters for a hydraulic power take-off unit of a wave energy converter in regular waves," *Proceedings of the Institution of Mechanical Engineers, Part A: Journal of Power and Energy*, vol. 226, no. 1, pp. 98–111, 2012.
[24] I. E. Commission *et al.*, "IEC TS 62600-2: 2019," *Technical Report*, 2019.
[25] A. Babarit, J. Hals, M. J. Muliawan, A. Kurniawan, T. Moan, and J. Krokstad, "Numerical benchmarking study of a selection of wave energy converters," *Renewable energy*, vol. 41, pp. 44–63, 2012.
[26] J. Falnes and M. Perlin, "Ocean waves and oscillating systems: Linear interactions including wave-energy extraction," *Applied Mechanics Reviews*, vol. 56, no. 1, p. B3, 2003.